

Noise Characterization in BeiDou-3 Multi-Frequency Observables

Robert Galatiya SUYA, Yung-Tsang CHEN, Chiew-Foong KWONG, Penghe ZHANG

Keywords: Noise Characterization, BeiDou-3, Multi-Frequency Observables, Precise Point Positioning, Modernized signals

SUMMARY

The booming number of BeiDou Navigation Satellite System (BDS)-3 satellites, improvements in satellite technology, and signal designs are persistently expanding the Global Navigation Satellite System (GNSS) domains of application. With the modernization of BDS, multiple satellites broadcast new frequencies and signals which are necessary for precise point positioning (PPP) performance. In this study, the noise characteristics of BDS-3 signals are investigated alongside that of the Global Positioning System (GPS) and Galileo (GAL). Moreover, the paper evaluates the contribution of interoperable signals to PPP performance. The results indicate that the noise in BDS-3 modernized signals is comparable to that of the other navigation systems. In the case of PPP, BDS-3 positioning performance is noticeably improved as a result of adding GPS and GAL constellations. Thus, the less noisy BDS-3 signals could have a positive impact on PPP as the tracking stations with such signals densify.

Noise Characterization in BeiDou-3 Multi-Frequency Observables

Robert Galatiya SUYA, Yung-Tsang CHEN, Chiew-Foong KWONG, Penghe ZHANG

1 INTRODUCTION

The third-generation Beidou Navigation Satellite System (BeiDou-3, or simply BDS-3) has been providing positioning, navigation, and timing (PNT) services since July 2020. BDS-3 is a multi-constellation global navigation satellite system (GNSS) comprising satellites in three distinct orbits, namely the Medium Earth orbit (MEO), Geostationary Earth Orbit (GEO), and Inclined Geo-Synchronous (IGSO) orbit. Manufactured by the China Academy of Space Technology (CAST) and the Shanghai Engineering Center for Microsatellites (SECM), the satellites in these orbits transmit multi-frequency signals which are made available using a civilian GNSS receiver. For instance, the BDS-3 MEO and IGSO satellites transmit six navigation signals whereas their counterpart GEO satellites transmit only two signals. Table 1 summarises the BDS-3 signals and their corresponding observation codes. For B1I and B3I signals, the three letters (I, Q, and X) tagged to the numbers observation codes denote the in-phase (I), quadrature (Q), and the combination of both (in-phase and quadrature) channels, respectively. For the other signals, D and P denote data and pilot codes, respectively, whereas both X and Z denote the combination of data and pilot codes.

Table 1.1: Overview of BDS-3 service signals as of March 2022.

Frequency	Observation Codes			MEO	IGSO	GEO	Compatibility
B1I	2I	2Q	2X	✓	✓	✓	B1 (BDS-2)
B3I	6I	6Q	6X	✓	✓	✓	B3 (BDS-2)
B1C	1D	1P	1X	✓	✓	-	L1 and E1 (GPS and GAL)
B2a	5D	5P	5X	✓	✓	-	L5 and E5a (GPS and GAL)
B2b	7D	7P	7Z	✓	✓	-	E5b (GAL)
B2a+b	8D	8P	8X	✓	✓	-	E5a+b (GAL)

Further to that, the BDS-3 B1I and B3I signals are compatible with the legacy B1I and B3I signals for the BDS-2 constellation. In addition, the B1C signal overlaps the L1 and E1 signals for global positioning system (GPS) and Galileo (GAL) constellations, respectively. The B2a signal overlaps the L5 and E5a signals for GPS Block IIF and GAL satellites, respectively. Moreover, the B2b and B2a+b signals are interoperable with the GAL E5b and E5a+b signals, respectively. This form of flexibility in BDS-3 signals, with respect to other GNSS frequencies, offers room for integrated PNT solutions using multiple satellites from different GNSS. Within an individual navigation system, the multi-signal frequencies also facilitate the formulation of

observables with favorable low noise. The code and phase observables are affected by both systematic biases and random noise. By forming mathematical and stochastic models, one can determine the level of noise from different positioning models. Further details about noise amplification in GNSS positioning models can be found in Xu and Xu (2016).

According to studies by Vaclavovic and Dousa (2016) and Suya et al. (2021), pseudorange (code) multipath and noise are important elements in the characterization of the quality of code observables. Besides that, as noted by Amiri-Simkooei et al. (2016), the multipath and noise information is also valuable for developing stochastic models for precise point positioning (PPP) ambiguity resolution. Several studies have been undertaken to assess the characteristics of BDS-3 signals and their impact on positioning solutions. Yang et al. (2018) analyzed the BDS-3 signal quality and positioning accuracy using five experimental satellites. Zhang et al. (2019) evaluated the signal quality and the positioning performance of the BDS-3 constellation in comparison with BDS-2, GPS, and GAL satellites. Wanninger and Beer (2015) identified elevation-dependent systematic biases larger than a meter in BDS MEO and IGSO code observations. In their study, a noticeable negative effect was also observed on the single-frequency PPP solution. Similarly, Zhang et al. (2017) observed that the systematic biases induce code-phase divergences and strong systematic variations in the time series.

In addition, according to Nie et al. (2018), a comparison in signal strength between BDS-2 and BDS-3 satellites indicated that the latter had a better signal quality than the former due to more stable time and frequency standards. Taking advantage of this quality, Geng and Guo (2020) undertook a PPP experiment with ambiguity resolution which showed that the BDS-3 signals such as B1C/B3I/B2a can suppress phase noise amplification for the processing model and in turn lead to improved positioning accuracy. Considering different GNSS constellations, Roberts (2019) evaluated the relative noise for different frequencies, orbit types, and satellite generation. In that study, only BDS-2 observations were involved and more noise was revealed in the B1I signal on BDS-2 MEO satellites. By considering BDS-2 and BDS-3 satellites, Yang et al. (2018) observed similar code noise accuracy for the same types of satellites.

Currently, multiple BDS-3 satellites broadcast modernized signals which are imperative in satellite-based positioning. Considerable research work on noise characterization is mainly based on BDS-2 only or in comparison with other GNSS. This paper investigates the noise characteristics of BDS-3 signals in comparison with their counterpart interoperable signals for GPS and GAL satellite systems. Moreover, the paper further explores the contribution of the compatible signals of BDS-3, GPS, and GAL constellations on PPP performance.

2 NOISE CHARACTERIZATION

2.1 Multipath Interference

The multipath interference occurs when the GNSS receiver receives reflected signals in addition to the line-of-sight (LOS) signals from the satellite. Signals at low elevation mask are usually susceptible to severe multipath effects due to different reflecting objects in the receiver environment. The multipath takes different names, for example, multipath affecting pseudorange and carrier-phase observations are termed code and phase multipath, respectively. The code multipath has a significant contribution to pseudorange-based positioning such as navigation, single point positioning (SPP), or PPP (Kaplan & Hegarty, 2017).

BDS-3 signals implement different modulation schemes, and as such, they are expected to demonstrate different multipath effects. For BDS-3 signals, the multipath combination of pseudorange and phase observations can be expressed using the geometry-free and ionosphere-free equation as in Vaclavovic & Dousa (2016):

$$\left. \begin{aligned} MP_k &= P_k - \Phi_i - \beta(\Phi_i - \Phi_j) \\ &= P_k + \alpha\Phi_i + \beta\Phi_j \end{aligned} \right\} \quad [2.1]$$

with

$$\left. \begin{aligned} \alpha &= \frac{f_i^2(f_k^2 + f_j^2)}{f_k^2(f_i^2 - f_j^2)} \\ \beta &= \frac{f_j^2(f_k^2 + f_i^2)}{f_k^2(f_i^2 - f_j^2)} \end{aligned} \right\}$$

where MP_k denotes the code multipath; P and Φ denote the code and phase observations, respectively; α and β denote the frequency combination scalars; λ denotes the wavelength; the subscripts i , j , and k denote frequency indices. It is worth noting that multipath values are manifested as variation over the continuous ambiguity block, and these changes reflect the multipath effects and pseudorange noise. Moreover, the tropospheric, ionospheric, and geometric errors are differenced out in equation [2.1]; and f denotes the frequency.

2.2 Signal-to-noise Ratio

The signal-to-noise ratio (SNR) is one parameter used for defining the quality of a GNSS signal. The receiver environment may have different reflecting objects which generate the stochastic signals within the receiver-satellite geometry. The stochastic signals impair the acquisition and tracking capabilities of the GNSS receiver. For each satellite in view, the receiver outputs the SNR in dBHz as a ratio between the desired signal power to the background noise power. Specifically, the SNR approximates the carrier-to-noise-density ratio (C/N_0) to the weighted

noise power spectral density (Strode & Groves, 2016). The C/N_0 is simply the ratio of the carrier power (C) to the noise power density (N_0). For signals contaminated with multipath, the C/N_0 is always lower than that of direct signals. Therefore, the SNR can be used to measure multipath contamination of a GNSS signal.

2.3 Precise Point Positioning Validation

The phase and code are the basic observations required in satellite-based positioning. This paper evaluates the PPP performance using the compatible signals between BDS-3, GPS, and GAL. Given phase and code observations, the GNSS observational function can be expressed as Leick et al. (2015):

$$\begin{cases} \Phi_{m,r}^s = \rho_r^s + c(\Delta t_r - \Delta t^s) - \mu_m I_r^s + \zeta_{m,r} - \zeta_m^s + \lambda_m N_{m,r}^s + \epsilon_{m,r}^s \\ P_{m,r}^s = \rho_r^s + c(\Delta t_r - \Delta t^s) + \mu_m I_r^s + \delta_{m,r} - \delta_m^s + \epsilon_{m,r}^s \end{cases} \quad [2.2]$$

where $\Phi_{m,r}^s$ and $P_{m,r}^s$ denote the phase and code measurements, respectively; r and s denote the receiver and satellite, respectively; m denotes GNSS carrier frequency ($m = 1, 2$); ρ_r^s denotes the geometric distance including the slant tropospheric delay and antenna phase center variation (PCV) and offsets (PCO) errors; c denotes the speed of light in a vacuum; Δt_r and Δt^s denote the receiver and satellite clock offset, respectively; μ_m denotes the coefficient for the signal; I_r^s denotes the slant ionospheric delay; λ_m denotes the phase wavelength; $N_{m,r}^s$ denotes the carrier phase integer ambiguity; $\zeta_{m,r}$ and $\delta_{m,r}$ denote receiver hardware biases on code and phase, respectively, ζ_m^s and δ_m^s denote satellite hardware biases on code and phase, respectively; $\epsilon_{m,r}^s$ and $\epsilon_{m,r}^s$ denote the code and phase noise, respectively.

The ionosphere is one of the main sources of error in GNSS that degrades positioning performance. To eliminate the first-order ionospheric delay, the ionosphere-free (IF) linear combination observable is formulated as follows

$$\begin{cases} \Phi_{IF,r}^s = \rho_r^s + c(\Delta t_r - \Delta t^s) + \zeta_{IF,r} - \zeta_{IF}^s + \lambda_1 N_{IF,r}^s + \epsilon_{IF,r}^s \\ P_{IF,r}^s = \rho_r^s + c(\Delta t_r - \Delta t^s) + \delta_{IF,r} - \delta_{IF}^s + \epsilon_{IF,r}^s \end{cases} \quad [2.3]$$

3 EXPERIMENTAL DESIGN

A total of seventeen (17) globally distributed stations were selected for the experiment as shown in Figure 3.1. All the stations (red) were used for the evaluation of noise in terms of SNR and multipath, while thirteen (13) stations (blue) were used for PPP validation. For all the stations, seven (7) days of datasets spanning from the day of year (DOY) 060 to 066 in 2022 (March 1 to 7, 2022) were used. The code multipath and SNR for BDS-3 signals were evaluated in comparison with those of GPS (L1 and L5), and GAL (E1 and E5a).

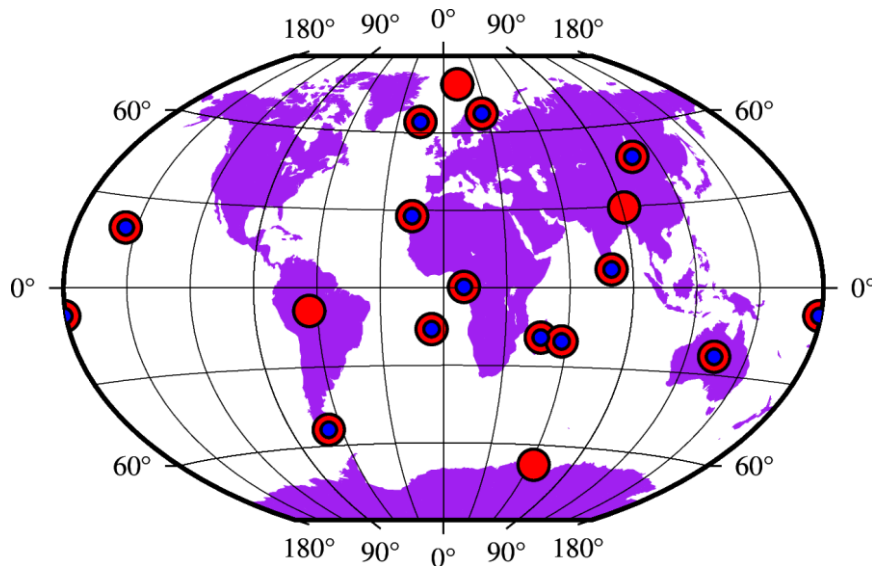


Figure 3.1: Distribution of the GNSS tracking stations for data processing.

The 13 stations for the PPP test were selected because, they can track the B1C/B2a, L1/L5, and E1/E5a for BDS-3, GPS, and GAL, respectively. The remaining four stations were excluded from the experiment because they do not track the BDS-3 B1C and B2a signals. As mentioned in Section 1 (Table 1.1), these signals are compatible between the three satellite systems, and were used to analyze the BDS-3 and the triple-constellation PPP performance consisting of BDS-3, GPS, and GAL satellites. The orbits and clocks were corrected using the WUM0MGXFIN products generated by Wuhan University. Also known as WUM, WUM0MGXFIN is a product identity, and one of the multi-GNSS experiment (MGEX) products in the form of satellite, clock, and earth rotation parameters for all GNSS including GPS, GLONASS (Globalnaya Navigazionnaya Sputnikovaya Sistema, or simply Global Navigation Satellite System), GAL, BDS-2, BDS-3, and QZSS (Quasi-Zenith Satellite System). Further details about WUM0MGXFIN can be found in Suya et al. (2022). The phase and code standard deviations were set at 0.006 cycles and 300 mm, respectively. The PCO and PCV, sagnac effect, phase wind-up, relativistic effect, tidal displacement, and tropospheric delay were also accounted for. Table 3.1 shows the PPP data processing strategies.

Table 3.1: PPP processing criteria.

Parameter	Strategy
Program	Least-squares
Tracking datasets	Fifteen globally distributed stations (Figure 3.1)
Sampling	30 seconds
Constellation	BDS-3, GPS, GAL
Signal Combination	B1C/B2a, L1/L5a, E1/E5a
MGEX product	WUM0MGXFIN
Cut-off Angle	10°
Weighting	Phase = 0.006 cycles; Code = 300 mm;
PCO and PCV	Corrected with igs14.atx
Sagnac effect	Corrected (Petit & Luzum, 2010a)
Phase wind-up	Corrected (Wu, Wu, Hajj, Bertiger, & Lichten, 1992)
Relativistic effect	Corrected (Kouba, 2009)
Tidal displacement	Applied (Petit & Luzum, 2010b)
Tropospheric delay	Saastamoinen model (Saastamoinen, 1972); estimated hourly using the Global Mapping Function (GMF, Boehm, Niell, Tregoning, & Schuh, 2006)
Station Coordinates	Estimated as constant
Ambiguity	Floating solution

4 RESULTS AND DISCUSSIONS

4.1 Code Multipath

The SNR and pseudorange multipath BDS-3, GAL, and GPS signals were estimated, and their mean solutions are presented in Figure 4.1. In this figure, three different colours are used to distinguish between the different observation codes between BDS-3, GAL, and GPS signals. Blue, red, and magenta colour are the bins for BDS-3, GAL, and GPS observation codes, respectively. For the 17 stations, all the available BDS-3 signals were considered in the experiment, and their pseudorange multipath is generally less than 40 cm except for the BDS-3 5X and 5P signals which have code multipath effects of about 40 cm (as shown in the upper panel). In the case of GAL signals, the code multipath is above 40 cm for all the observation codes with that of the 8X signal for E5(E5a+b) reaching up to about 48 cm. On the contrary, the GPS signals are less affected by code multipath for the selected stations, on both L1 and L5 signals. The difference in the multipath effects among the codes for the three satellite systems may be attributed to signal reflectors in the receiver environment. In addition, the disparity in noise and multipath may also be due to different transmission power and chip rate for the signals broadcast by BDS-3, GAL, and GPS. For example, the GPS L5 signal (5Q and 5X) has a higher

transmission power and chip rate than the legacy L1 C/A code (1C) signal (Circiu, Felux, & Pullen, 2015). Moreover, the GAL binary offset carrier (BOC) signal of 1C exhibits higher multipath and noise despite its higher chip rate and noise signal power than the GPS 1C signal. It is worth mentioning that the GAL 1C signal is modulated through the Binary Phase-Shift Keying (BPSK) just like the BDS-3 B1 signal. Further details about the BDS-3 modulation schemes and chip rate can be found in Suya et al. (2021).

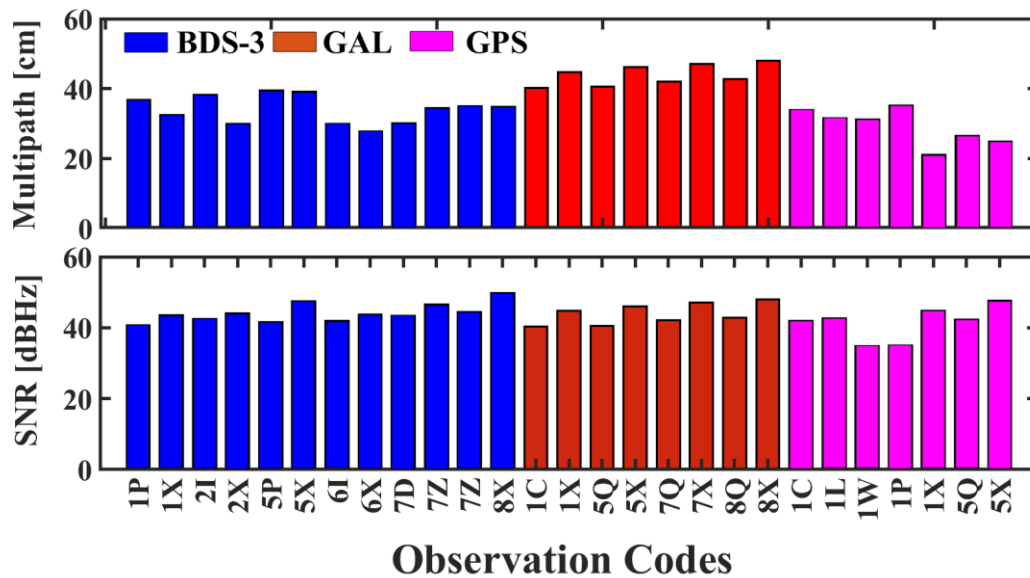


Figure 4.1: Pseudorange multipath and SNR comparison between BDS-3, GAL, and GPS signals.

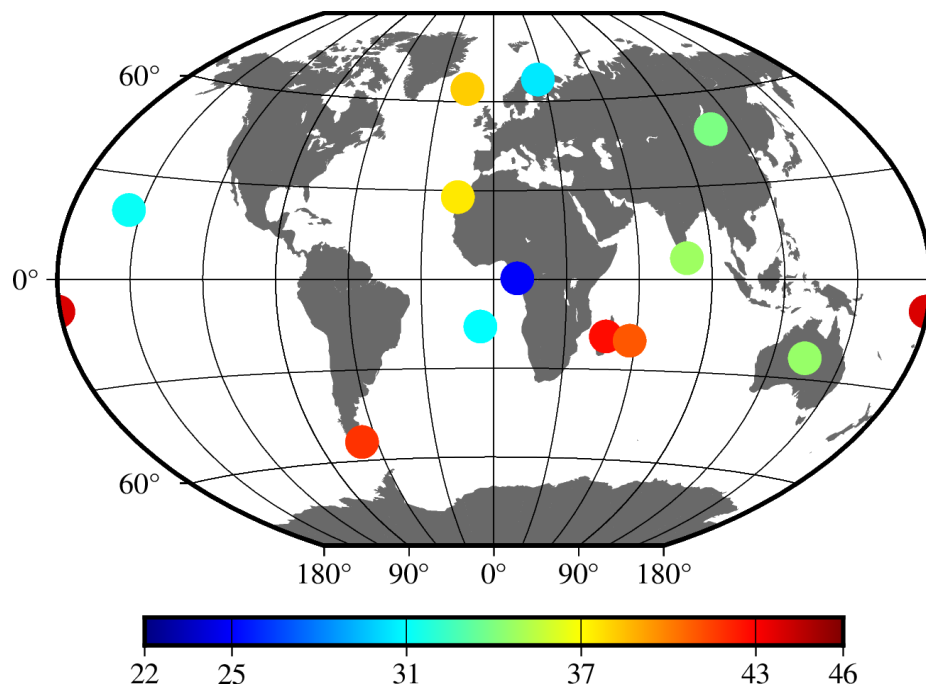


Figure 4.2: BDS-3 code multipath for B1C signal (cm).

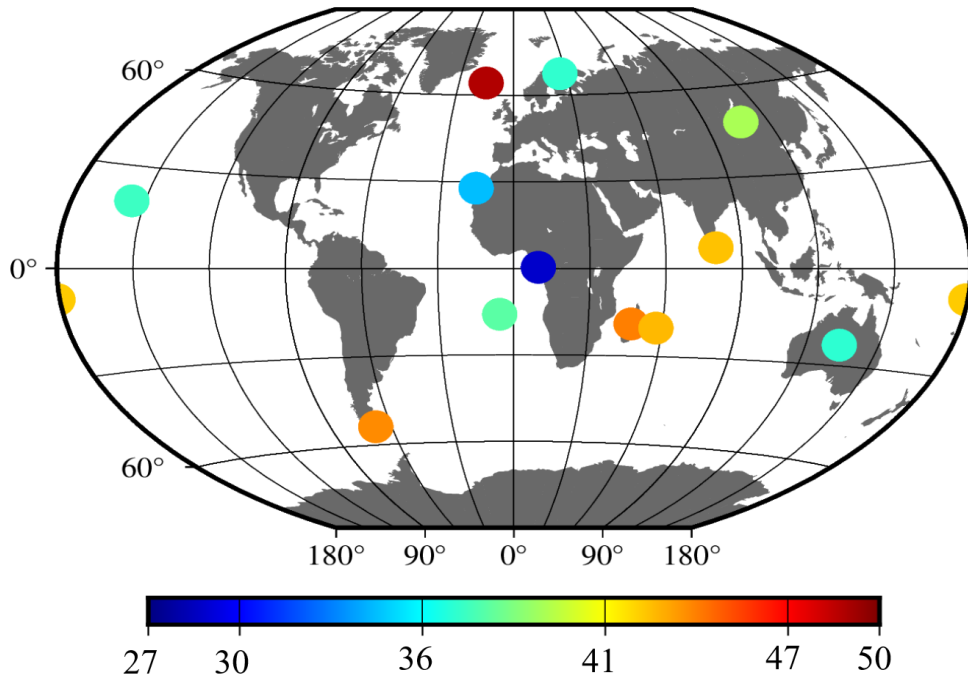


Figure 4.3: BDS-3 code multipath for B2a signal (cm).

To further classify the code multipath effects for BDS-3 signals, the estimated solutions were superimposed on the stations with B1C/B2a tracking capability. Figures 4.2 and 4.3 illustrate the BDS-3 code multipath on the BC1 and B2a signals. As can be seen, the multipath effects are in the range of 22 to 46 and 27 to 50 cm for B1C and B2a signals, respectively.

4.2 SNR

To extend the characterization of the signals, the SNR for the three selected signals is compared in Figure 4.1 (lower panel). As explained in Section 2.2, the SNR is used to characterize the magnitude of the C/N_0 for GNSS signals. As can be evidenced from Figure 4.1, the SNR for all navigation systems is generally above 40 dBHz, except for GPS 1W and 1P codes which are about 35 dBHz. The numerical statistics for both the multipath and SNR are summarized in Table 4.1. From this table, the BDS-3 8X signal (B2a+b) has a SNR reaching up to about 50 dBHz, followed by its compatible GAL 8X signal (about 48 dBHz). Similarly, the GPS 5X signal exhibits a similar magnitude to that of the GAL 8X signal. Further to that, the 5X and 7X signals for BDS-3 and GAL both have a signal strength of about 47 dBHz. In a suitable environment, the GNSS receiver should output a SNR of not less than 42 dBHz (Strode & Groves, 2016). In this research, 93% of the estimated signals are within the acceptable ranges (42 dBHz) for an ideal receiver. Figures 4.4 to 4.6 compare the SNR for 1X signal for BDS-3

(B1C), GAL (E1), and GPS (L1C) constellations using five GNSS stations namely, BRST, ENAO, ULAB, WIND, and WUH2 on DOY 060 in 2022. At all the stations, the SNR at lower elevations is generally noisier than at higher elevations denoting susceptibility to multipath effects and noise.

Table 4.1: Averaged multipath and SNR statistics for BDS-3, GAL, and GPS signals.

BDS-3 signals	1P	1X	2I	2X	5P	5X	6I	6X	7D	7Z	7Z	8X
Multipath (cm)	36.76	32.53	38.24	29.84	39.51	39.15	29.98	27.8	30.10	34.49	35.00	34.86
SNR (dBHz)	40.70	43.62	42.41	44.04	41.58	47.46	42.01	43.7	43.34	46.57	44.41	49.79
Galileo signals	1C	1X	5Q	5X	7Q	7X	8Q	8X				
Multipath (cm)	40.27	44.73	40.52	46.11	42.09	47.05	42.80	47.98				
SNR (dBHz)	40.27	44.73	40.52	46.11	42.09	47.05	42.80	47.98				
GPS signals	1C	1L	1W	1P	1X	5Q	5X					
Multipath (cm)	33.93	31.57	31.15	35.16	21.03	26.39	24.77					
SNR (dBHz)	41.94	42.60	34.85	35.05	44.75	42.25	47.67					

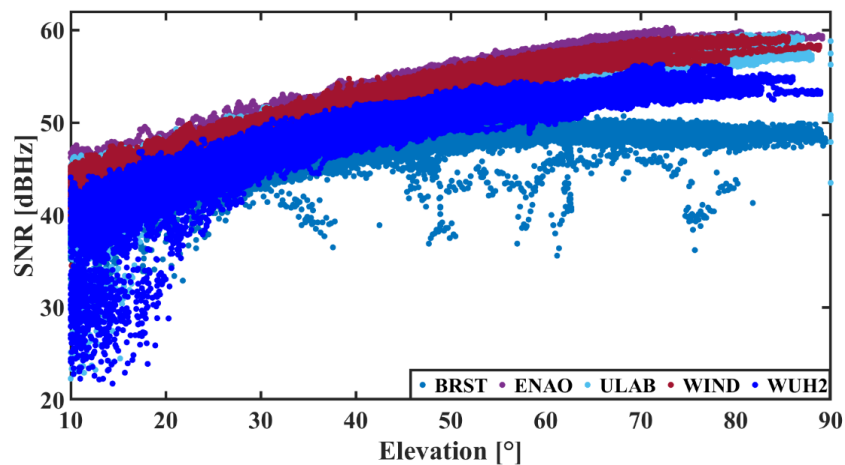


Figure 4.4: SNR for BDS-3 1X signal.

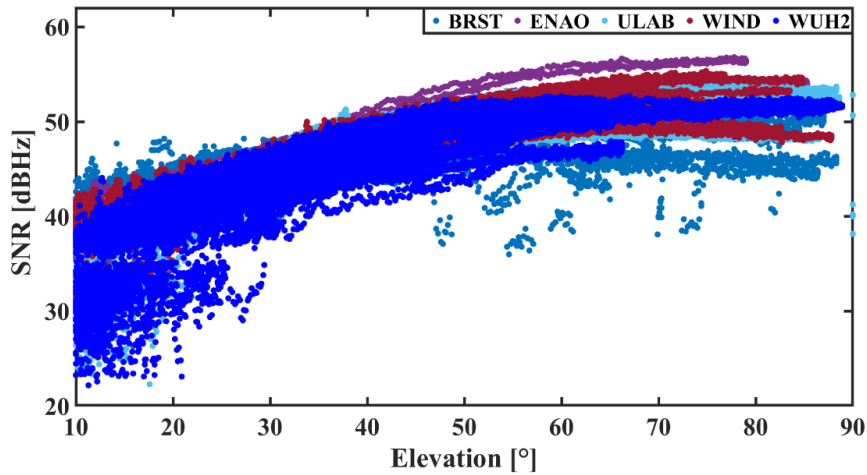


Figure 4.5: SNR for GAL 1X signal.

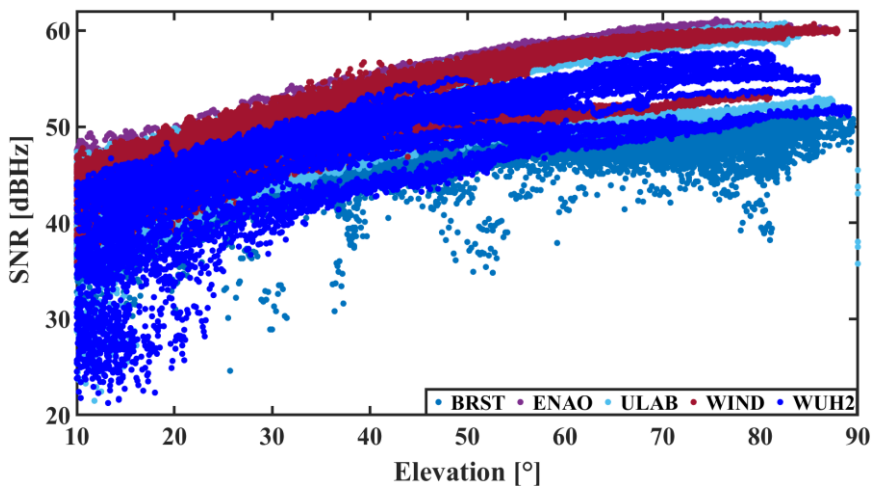


Figure 4.6: SNR for GPS 1X signal.

4.3 PPP

To evaluate the contribution of BDS-3/GPS/GAL interoperable signals on PPP, 13 MGEX stations with observations for the aforementioned constellations were utilized. Figure 4.7 shows the kinematic PPP solution for the selected stations from DOY 060 to 066 in 2022. The upper and lower panels depict the PPP performance in the North, East, and Up components for BDS-3 and BDS-3+GPS+GAL constellations, respectively. The different colours denote the standard deviations for the selected stations during the experiment period. On each DOY, the first bins denote the mean solutions, whereas the second, third, and fourth denote the 25th, 50th, and 75th percentiles, respectively.

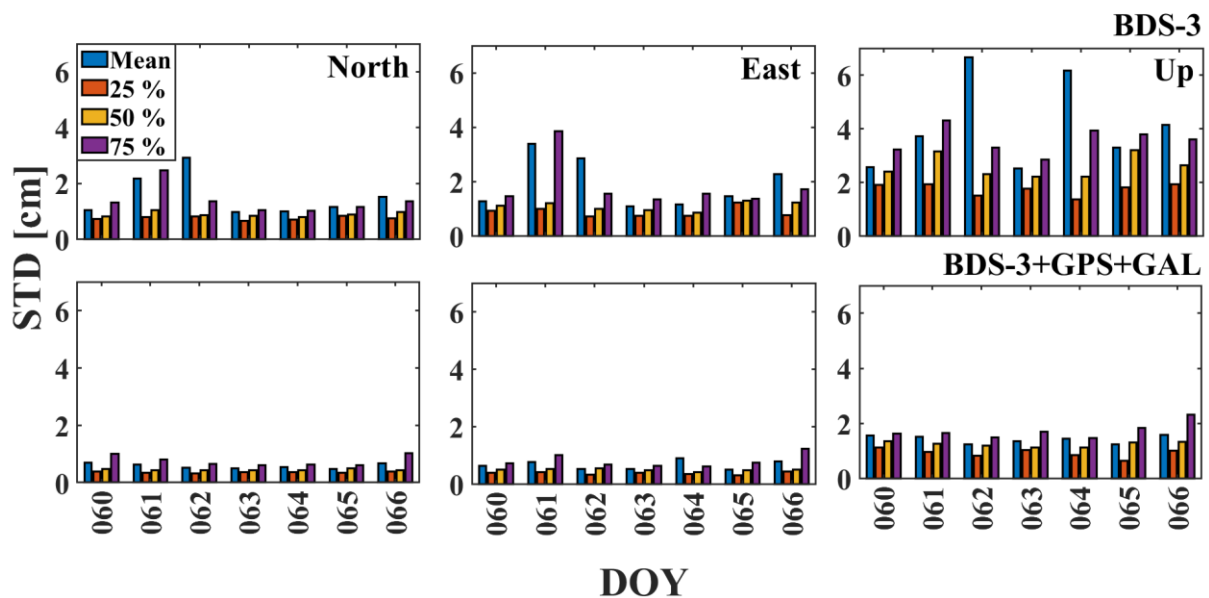


Figure 4.7: PPP performance in North, East, and Up components.

For the BDS-3, the PPP performance in all components is generally less than 4 cm except for 57% of results in the vertical component on four days (DOY 061, 062, 064, and 066). On average, the mean standard deviations in the North, East, and Up components are about 1.55 cm, 1.94 cm, and 4.58 cm, respectively. In comparison with the integrated positioning in the lower panel (Figure 4.7), there is an apparent improvement in the performance in all three directions. Specifically, the positioning performance in the combined solution is pegged at 0.59 cm, 0.67 cm, and 1.42 cm in the North, East, and Up directions, respectively. This change indicates an improvement of 62% (from 1.55 to 0.59 cm), 65% (from 1.94 to 0.67 cm), and 69% (from 4.58 to 1.42 cm) in the North, East, and Up directions, respectively. Table 4.2 compares the numerical statistics for PPP performance in North, East, and Up components between BDS-3 and BDS-3+GPS+GAL constellations. The numbers enclosed in brackets indicate the improvement (in percent) in BDS-3 PPP performance as a result of adding GPS and GAL satellite systems. Despite the limited number of stations used to evaluate the PPP performance, the results demonstrate that cm-level accuracy can be achieved with BDS-3 only B1C/B2a signals.

Table 4.2: Numerical statistics for PPP performance in North, East, and Up components.

	Mean (cm)	25%	50%	75%	Remark
BDS-3	1.55	0.76	0.90	1.40	North
	1.94	0.89	1.11	1.85	East
	4.58	1.76	2.60	3.58	Up
BDS-3+GPS+GAL	0.59 (62)	0.38 (50)	0.47 (48)	0.78 (44)	North
	0.67 (65)	0.39 (56)	0.51 (54)	0.82 (56)	East
	1.42 (69)	0.93 (47)	1.25 (52)	1.74 (51)	Up

5 CONCLUSIONS

This study focused on noise characterization for BDS-3 multi-frequency signals using observations from globally distributed stations. The code multipath and SNR for BDS-3 signals were evaluated in comparison to those of GPS and GAL. The results demonstrated that multipath effects and SNR were comparable between the three navigation systems. Moreover, the kinematic PPP performance using the interoperable signals indicated that the BDS-3 constellation can achieve cm-level precision in the daily solutions. The positioning accuracy further improved when BDS-3 was extended to the multi-constellation and multi-frequencies by adding GPS and GAL systems. Therefore, BDS-3 PPP may benefit from the less noisy and modernized signals broadcast by GPS and GAL satellites. This research, however, did not consider other signals for GPS and GAL, and the next research direction will dwell on all the signals using short and zero baseline tests.

ACKNOWLEDGEMENTS

Noise Characterization in BeiDou-3 Multi-Frequency Observables (11516)
 Robert Galatiya Suya, Yung-Tsang Chen, Chiew-Foong Kwong and Penghe Zhang (China, PR)

FIG Congress 2022
 Volunteering for the future - Geospatial excellence for a better living
 Warsaw, Poland, 11–15 September 2022

The authors would like to express their gratitude to the International GNSS Service for publicly sharing their data. This work is supported by Ningbo Science and Technology Bureau under Commonweal Research Program with project code 2019C50017 and a research grant with project code A0060 from Ningbo Nottingham New Material Institute.

5 REFERENCES

- Amiri-Simkooei, A. R., Jazaeri, S., Zangeneh-Nejad, F., & Asgari, J. (2016). Role of stochastic model on GPS integer ambiguity resolution success rate. *GPS Solutions*. <https://doi.org/10.1007/s10291-015-0445-5>
- Boehm, J., Niell, A., Tregoning, P., & Schuh, H. (2006). Global Mapping Function (GMF): A new empirical mapping function based on numerical weather model data. *Geophysical Research Letters*, 33(7). <https://doi.org/10.1029/2005GL025546>
- Circiu, M. S., Felux, M., & Pullen, S. (2015). Galileo E1 and E5A performance: For Multi-Frequency, Multi-Constellation GBAS. *GPS World*, 26(4), 30–35.
- Geng, J., & Guo, J. (2020). Beyond three frequencies: an extendable model for single-epoch decimeter-level point positioning by exploiting Galileo and BeiDou-3 signals. *Journal of Geodesy*, 94(1), 1–15. <https://doi.org/10.1007/s00190-019-01341-y>
- Kaplan, E. D., & Hegarty, C. J. (2017). Understanding GPS/GNSS Principles and Applications. In *GNSS Technology and Applications Series*. Norwood: Artech House.
- Kouba, J. (2009). A Guide to using international GNSS Service (IGS) Products. *Geodetic Survey Division Natural Resources Canada Ottawa*, 6, 34. Retrieved from <http://graypantherssf.igs.org/igsdb/resource/pubs/UsingIGSProductsVer21.pdf>
- Leick, A., Rapoport, L., & Tatarnikov, D. (2015). GPS Satellite Surveying: Fourth Edition. Wiley. <https://doi.org/10.1002/9781119018612>
- Nie, Z., Gao, Y., Wang, Z., Ji, S., & Yang, H. (2018). An approach to GPS clock prediction for real-time PPP during outages of RTS stream. *GPS Solutions*, 22(1), 1–14. <https://doi.org/10.1007/s10291-017-0681-y>
- Petit, G., & Luzum, B. (2010a). IERS Conventions (2010). IERS Technical Note 36. *Verlagdes Bundesamts Für Kartographie Und Geodäsie*.
- Petit, G., & Luzum, B. (2010b). IERS Conventions (2010). *Bureau International Des Poids Et Mesures Sevres (France)*.

- Roberts, G. W. (2019). Noise comparison of triple frequency GNSS carrier phase, doppler and pseudorange observables. *Measurement: Journal of the International Measurement Confederation*, 144, 328-344. <https://doi.org/10.1016/j.measurement.2019.05.011>
- Saastamoinen, J. (1972). Contributions to the theory of atmospheric refraction. *Bulletin Géodésique*. <https://doi.org/10.1007/BF02521844>
- Strode, P. R. R., & Groves, P. D. (2016). GNSS multipath detection using three-frequency signal-to-noise measurements. *GPS Solutions*. <https://doi.org/10.1007/s10291-015-0449-1>
- Suya, R. G., Chen, Y. T., Kwong, C.F. & Zhang, P. (2022). BeiDou intra-system bias using different precise orbit and clock products. *Measurement: Journal of the International Measurement Confederation*, 191(January), 110804. <https://doi.org/10.1016/j.measurement.2022.110804>
- Suya, R. G., Chen, Y. T., Kwong, C. F., Zhang, P., & Hancock, C. M. (2021). The contribution of BeiDou-3 binary offset carrier signals to single point positioning. *FIG E-Working Week 2021 Smart Surveyor for Land and Water Management - Challenges in a New Reality, 21–25 June 2021*. Retrieved from https://fig.net/fig2021/technical_program.htm
- Vaclavovic, P., & Dousa, J. (2016). G-nut/Anubis: Open-source tool for multi-GNSS data monitoring with a multipath detection for new signals, frequencies and constellations. *International Association of Geodesy Symposia*. https://doi.org/10.1007/1345_2015_97
- Wanninger, L., & Beer, S. (2015). BeiDou satellite-induced code pseudorange variations: diagnosis and therapy. *GPS Solutions*. <https://doi.org/10.1007/s10291-014-0423-3>
- Wu, J. T., Wu, S. C., Hajj, G. A., Bertiger, W. I., & Lichten, S. M. (1992). Effects of antenna orientation on GPS carrier phase. *Astrodynamics 1991*. 1647-1660.
- Xu, G., & Xu, Y. (2016). *GPS: Theory, algorithms and applications*, Third Edition. <https://doi.org/10.1007/978-3-662-50367-6>
- Yang, Y., Xu, Y., Li, J., & Yang, C. (2018). Progress and performance evaluation of BeiDou global navigation satellite system: Data analysis based on BDS-3 demonstration system. *Science China Earth Sciences*. <https://doi.org/10.1007/s11430-017-9186-9>
- Zhang, X., He, X., & Liu, W. (2017). Characteristics of systematic errors in the BDS Hatch–Melbourne–Wübbena combination and its influence on wide-lane ambiguity resolution. *GPS Solutions*, 21(1), 265–277. <https://doi.org/10.1007/s10291-016-0520-6>
- Zhang, Z., Li, B., Nie, L., Wei, C., Jia, S., & Jiang, S. (2019). Initial assessment of BeiDou-3

global navigation satellite system: signal quality, RTK and PPP. *GPS Solutions*.
<https://doi.org/10.1007/s10291-019-0905-4>

CONTACTS

Mr. Robert Galatiya Suya
University of Nottingham Ningbo China, 199 Taikang East Road, 315100, Ningbo, China.
Email: robert.suya@nottingham.edu.cn

Dr. Yung-Tsang Chen
University of Nottingham Ningbo China, 199 Taikang East Road, 315100, Ningbo, China.
Email: yung-tsang.chen@nottingham.edu.cn

Dr. Chiew-Foong Kwong
University of Nottingham Ningbo China, 199 Taikang East Road, 315100, Ningbo, China
Email: chiew-foong.kwong@nottingham.edu.cn

Dr. Penghe Zhang
Motovis Intelligent Technologies (Shanghai) Co., Ltd, P.O Box 201203, China
Email: penghezhang@hotmail.com